

## A NEW APPROACH TO DETERMINE AND EVALUATE THE POISSON'S RATIO OF WOOD

Klara Winter<sup>1</sup>, Roland Maderebner<sup>2</sup>, Philipp Dietsch<sup>3</sup>

**ABSTRACT:** Modern timber engineering requires increasing application of the finite element method (FEM). In such analyses, the elastic constants including the Poisson's ratios are required. The latter have mostly been neglected so far, since these vary to a great degree in related literature. Hence, an experimental method based on compression tests was developed and benchmarked on numerous preliminary tests in order to determine the Poisson's ratios on spruce wood (*Picea Abies*). For the first time, the extended measurement uncertainty was taken into account. On the basis of these values, a comparison with values from literature was conducted. Several observations indicate that, in addition to the wood properties, the load application as well as the test setup have a significant influence on the Poisson's ratios. In summary, all obtained values lie in the medium range of the literature values. Consequently, the developed test method for determining the Poisson's ratios is considered to be suitable. In addition, an expanded Poisson's ratio was determined taking into account the measurement uncertainty in order to obtain a symmetrical compliance matrix.

**KEYWORDS:** Wood, Spruce (*Picea Abies*), Poisson's Ratios, FEM, Elastic behaviour, Measurement uncertainty

### 1 INTRODUCTION

For numerical calculation of increasingly complex timber structures and three-dimensional timber connections using the finite element method (FEM), the Poisson's ratios are required. When loading a body in its axial direction this measure indicates the ratio between lateral ( $\varepsilon_l$ ) and axial strain ( $\varepsilon_a$ ). The ratios published so far, vary greatly in their order of magnitude. Therefore, the Poisson's ratios are often neglected in numerical calculations. Moreover, numerous studies leave uncertainty, which and why a certain test method was applied.

In the context of this work, an own test procedure was developed to clarify, what influences the Poisson's ratios and what causes the great deviation in the published values. Within this process, the most suitable out of three available measurement techniques was selected. Depending on the measurement technique and the test procedure the extended measurement uncertainty was calculated as well. Thus, a range, in which the true mean value of the determined Poisson's ratio lies can be stated with a confidence of approx. 95 %. Moreover, computer tomography (CT) measurements were conducted to verify the linear elastic range.

Although there are several different wood species, this study only refers to spruce wood, as this, together with fir, makes up the largest share of construction timber in Central Europe.

Preliminary literature on determining the Poisson's ratios predominantly applied tensile tests (e.g. [1]-[7]). For the sake of simplicity and as is stated in [7] and [8] the load type was assumed to have no direct influence on the Poisson's ratio. Only compression tests were performed within this work.

### 2 MATERIALS AND METHODS

#### 2.1 WOODEN SPECIMENS

All measurements on wood were performed on spruce wood (*Picea*). The source of the wood was near Iseltal in Austria. The specimens were conditioned in a climate chamber at a temperature of  $(20 \pm 1)^\circ\text{C}$  and a relative humidity of  $(65 \pm 3) \%$  according to [9] and [10]. A total, of three different specimen groups (L, R and T) were prepared in order to perform the preliminary tests and main tests for all six Poisson's ratios. To achieve the most accurate results, the fibre orientation should be as parallel to the specimen axes as possible. Therefore, the maximum specimen length was examined on the available wood, without having to accept a strong deviation of the fibre orientations. This resulted in specimen dimensions of  $l \times h \times b = 100 \times 30 \times 30 \text{ mm}^3$  (Figure 1).

The specimen surfaces were sanded to straighten protruding fibres and saw edges. A total of a 150 specimens per specimen group were manufactured. In this way, it was ensured that enough test specimens were

<sup>1</sup> Klara Winter, Technical University of Munich, Germany,  
klara.winter@tum.de

<sup>2</sup> Roland Maderebner, Institute for Construction and Material Science, Unit of Timber Engineering, University of Innsbruck, Austria, roland.maderebner@uibk.ac.at

<sup>3</sup> Philipp Dietsch, Timber Structures and Building Construction, Karlsruhe Institute of Technology, Germany,  
dietsch@kit.edu

available for the preliminary tests and the 20 specimens for each Poisson's ratio for the main tests.

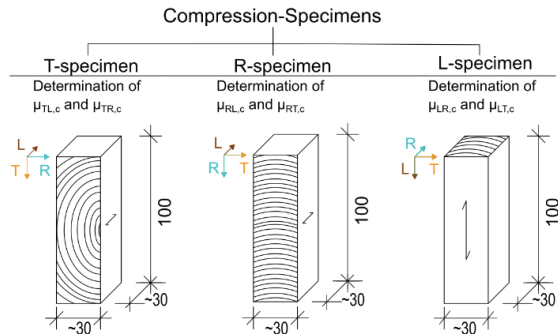


**Figure 1:** Different specimen groups including dimensions in [mm]

The test specimens had further to be pre-drilled on two opposite sides to realize the measurements using DD1 displacement and strain transducers (Figure 2).

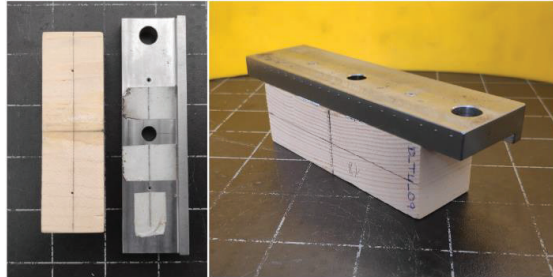


**Figure 2:** Metal drilling template on a wooden specimen; left: top view, right: side view

## 2.2 ALUMINIUM SPECIMEN

In addition to the wooden test specimens, an aluminium specimen was prepared. This was used as part of the preliminary tests to select the measurement. It was made of the material EN AW-2007-T4 and its dimensions were  $l \times h \times b = 100 \times 30 \times 30 \text{ mm}^3$ .

Like the wooden specimens, the aluminium specimen also had to be pre-drilled for the measurements using the strain gauged based DD1 displacement and strain transducers.

## 2.3 MEASUREMENT TECHNIQUE

The measurement technique was chosen based on comparative measurements preliminary to the main tests. In this regard, the most suitable out of three available measurement techniques including strain gauges, strain gauged based DD1 displacement and strain transducers and videoextensometry was to be selected. The repeatability was investigated by means of the aluminium specimen under compression. Aluminium was chosen as it was expected to not change its properties within the elastic range. The specimen was loaded eight times with each measurement technique. In between the individual loadings the aluminium specimen was removed and inserted into the testing machine again in order to simulate the subsequent test sequence on the wooden specimens as equal as possible. All measurement techniques led to

nearly the same average Poisson's ratio of  $\mu_{alu} = 0,356$  but showed significantly different scattering (Figure 3).

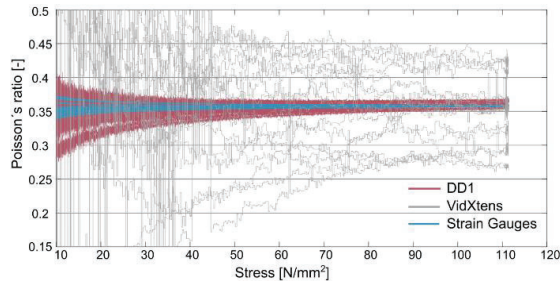


**Figure 3:** Comparison of the measurement signals obtained with the three measurement techniques on the aluminium specimen

The DD1 displacement and strain transducers showed a comparably good repeatability with a standard deviation of  $5,33 \cdot 10^{-3}$  and a CoV of 1,49 %. As these also required considerably less time for specimen preparation, this technique was chosen for all further measurements. In case of the measurements determining  $\mu_{RL}$  and  $\mu_{TL}$  a combination of both DD1 displacement transducers and strain gauges was applied. Reason for this are the significantly smaller lateral strains in grain direction that cause higher signal noise.

## 2.4 TEST SETUP USING DD1 DISPLACEMENT AND STRAIN TRANSDUCERS

A Shimadzu Autograph with an EDC 580 control unit from DOLI Elektronik GmbH was used for all measurements. A spherical cap and a steel cube on top of the wooden specimen ensured uniform load application within all tests (Figure 4).

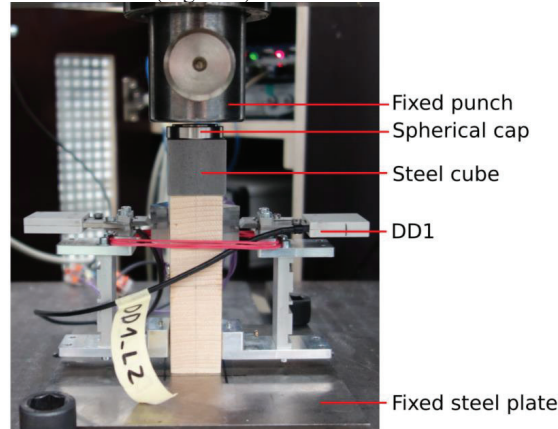


**Figure 4:** Load application and strain measurement using DD1 displacement and strain transducers

The lateral displacement in R- and T-direction could only be recorded using one DD1 displacement and strain transducer. In order to measure the axial displacement two DD1 were attached to opposite sides of the specimen (Figure 5). Thus, possible bending effects could be eliminated. The axial DD1 displacement transducers were attached to the specimen using small nails. Further, two

metal prisms were attached to the upper part of the specimen on opposite sides using small nails as well. The probe tips of the displacement transducers for the axial measurement were in contact with these. The distance between the nails and thus the initial length  $l$  was set to 60 mm.

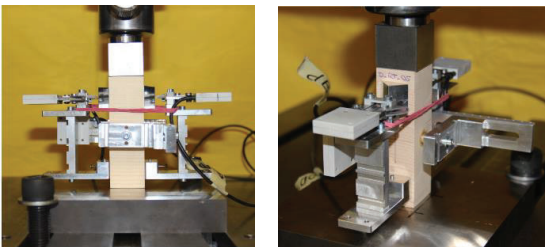


**Figure 5:** Test setup with DDI displacement and strain transducers on wooden specimen; left: Front view; right: Oblique view

Figure 6 shows the test setup for measuring  $\mu_{RL}$  and  $\mu_{TL}$ . For given reasons, two strain gauges were adhered on opposite sides of the specimen in order to measure the lateral displacement in grain direction.

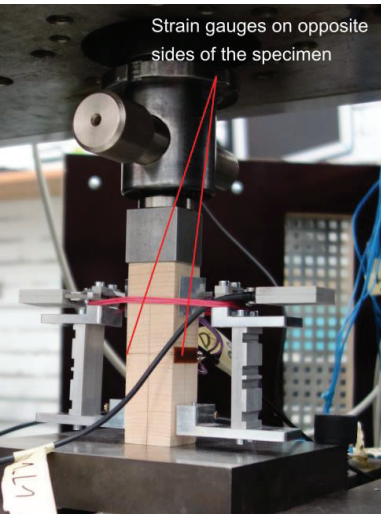


**Figure 6:** Measurement configuration used for determining  $\mu_{RL}$  and  $\mu_{TL}$

#### 2.4.1 Test procedure

All specimens were tested within one hour after removal from the climate chamber, as prescribed in [11]. Preceding the measurement, the specimens were prepared in the measurement room and the duration of the test itself was about 20 minutes. All tests were load-controlled, so that the theoretical compressive strength  $F_{c,max}$  would be reached in approx. 90 seconds [9]. Thus, the influence of creep deformations on the Poisson's ratio are eliminated. The load was applied in such a way that the test specimens were only loaded in their linear-elastic range. Hence, the upper load limit within the preliminary tests was set to 30 % of the compressive strength ( $f_{c,90,k}$  resp.  $f_{c,0,k}$ ) given in [12] for spruce wood of class C24. The maximum load applied within the main tests is derived from the CT

verification tests described in Section 3.1.3. All measurements were load controlled and started at a load level of 20 N.

Within the determination of the Young's modulus on concrete, this is loaded in several cycles. Thus, an initial and a stabilized Young's modulus is defined [13]. Following this procedure, measurements consisting of numerous loading and unloading cycles were performed.

#### 2.4.2 Three-dimensional Hooke's law for orthotropic materials

The three-dimensional Hooke's law is based on the assumption that stress  $\sigma_{ij}$  and strain  $\varepsilon_{kl}$  are linearly related. To describe the three-dimensional elastic behaviour of orthotropic materials 12 compliance coefficients  $S$  are necessary [14].

Furthermore, it is valid for orthotropic materials that shear stresses that act in the main direction do not generate normal strains. Normal stresses do not generate shear strains either. Moreover, shear strains are only generated by shear stresses in the same plane. [15] Several compliance parameters of orthotropic materials are therefore zero and the three-dimensional Hooke's law can be given in the following compliance form:

$$\begin{pmatrix} \varepsilon_1 \\ \varepsilon_2 \\ \varepsilon_3 \\ \gamma_{23} \\ \gamma_{13} \\ \gamma_{12} \end{pmatrix} = \begin{pmatrix} S_{11} & S_{12} & S_{13} & & & \\ S_{12} & S_{22} & S_{23} & & & \\ S_{13} & S_{23} & S_{33} & & & \\ & & & S_{44} & & \\ & & & & S_{55} & \\ & & & & & S_{66} \end{pmatrix} \cdot \begin{pmatrix} \sigma_1 \\ \sigma_2 \\ \sigma_3 \\ \tau_{23} \\ \tau_{13} \\ \tau_{12} \end{pmatrix} \quad (1)$$

where  $\varepsilon$  = strains [-],  $\gamma$  = shear strains [-],  $\sigma$  = normal stresses [ $N/mm^2$ ],  $\tau$  = shear stresses [ $N/mm^2$ ],  $S_{ii}$  for  $i = 1,2,3$ : Strain numbers [ $mm^2/N$ ],  $S_{ii}$  for  $i = 4,5,6$ : Shear strain numbers [ $mm^2/N$ ],  $S_{ij}$  for  $i,j = 1,2,3$ : Poisson's ratios;  $i \neq j$  [ $mm^2/N$ ].

Further, the compliance parameters can be replaced by the engineering parameters Young's modulus  $E$ , Shear modulus  $G$  and Poisson's ratio  $\mu$ . The indices can be replaced with the common labels L, R and T. Hooke's law then takes the form of Equation (2):

$$\begin{pmatrix} \varepsilon_{LL} \\ \varepsilon_{RR} \\ \varepsilon_{TT} \\ \gamma_{RT} \\ \gamma_{LT} \\ \gamma_{LR} \end{pmatrix} = \begin{pmatrix} \frac{1}{E_L} & -\frac{\mu_{RL}}{E_R} & -\frac{\mu_{TL}}{E_T} & & & \\ -\frac{\mu_{LR}}{E_L} & \frac{1}{E_R} & -\frac{\mu_{TR}}{E_T} & & & \\ -\frac{\mu_{LT}}{E_L} & -\frac{\mu_{RT}}{E_R} & \frac{1}{E_T} & & & \\ & & & \frac{1}{G_{RT}} & & \\ & & & & \frac{1}{G_{LT}} & \\ & & & & & \frac{1}{G_{LR}} \end{pmatrix} \cdot \begin{pmatrix} \sigma_{LL} \\ \sigma_{RR} \\ \sigma_{TT} \\ \tau_{RT} \\ \tau_{LT} \\ \tau_{LR} \end{pmatrix} \quad (2)$$

It is only applicable if the stresses and deformations are referred to the main axes [16]. If the main axes of the wood deviate from the reference system coordinate transformations as described e.g. in [14] and [17] must be applied.

The compliance matrix itself is symmetric. Due to this symmetry condition, only nine of the 12 parameters are independent of each other. It applies:

$$\frac{\mu_{LR}}{E_L} = \frac{\mu_{RL}}{E_R} \quad (3)$$

$$\frac{\mu_{LT}}{E_L} = \frac{\mu_{TL}}{E_T} \quad (4)$$

$$\frac{\mu_{RT}}{E_R} = \frac{\mu_{TR}}{E_T} \quad (5)$$

Further requirements for the compliance matrix are given in [16] and [2].

#### 2.4.3 Calculation of the Poisson's ratio

The Poisson's ratio describes the lateral contraction/elongation ( $\varepsilon_l$ ) of a body as it elongates or contracts normal to the force ( $\varepsilon_a$ ) (Equation (6)). Thus, it is also called passive deformation. The Poisson's ratio is always negative since compression is defined as negative tension.

$$\mu_{al} = -\frac{\varepsilon_l}{\varepsilon_a} \quad (6)$$

#### 2.4.4 Calculation of the Young's modulus

The Young's moduli  $E_{i,ij}$  were examined on the basis of the tenth loading and unloading cycle between 20 % and 55 % of the estimated upper load limit  $F_{c,max,est}$  using Equation (7):

$$E_{i,ij} = \frac{(\sigma_{i,55} - \sigma_{i,20}) \cdot 60mm}{\Delta l_{i,55} - \Delta l_{i,20}} \quad (7)$$

where  $i,j$  = Anatomical directions resp. load directions, each can attain independently L,R or T [-],  $\sigma_{i,20}$ ,  $\sigma_{i,55}$  = stress at 20 % resp. 55 % of  $F_{c,max,est}$  when loaded in i-direction [ $N/mm^2$ ],  $\Delta l_{i,20}$ ,  $\Delta l_{i,55}$  = Axial displacement in i-direction at 20 % resp. 55 % of  $F_{c,max,est}$ .

#### 2.4.5 Data processing

Within the scope of this work, the Poisson's ratios and Young's moduli were determined on the basis of several loading and unloading paths. However, due to the dissipated energy during specimen deformation, the paths individually would lead to varying results. This effect is called hysteresis [18]. Hence, these were averaged. Figure 7 shows this effect by means of a randomly selected loading and unloading path of a measurement on the aluminium specimen. This specimen was loaded and unloaded once in the stress range between 60 to 105  $N/mm^2$ . The red path, which is then used for further evaluation represents the average of the loading and the unloading path.

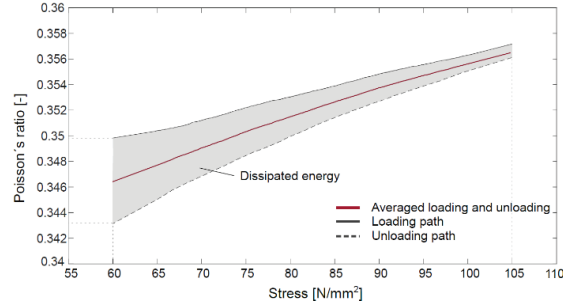


**Figure 7:** Hysteresis effect on the basis of a loading and unloading path of the aluminium specimen measured with the DDI displacement and strain transducers

Those measurements that still exhibited signal noise after averaging were further denoised, using the Savitsky-Golay filter.

#### 2.4.6 Determination of the measurement uncertainty

When specifying a physical variable, it is important to include the measurement uncertainty  $u(x)$ , as all measurement results include errors. The calculation of the measurement uncertainty is described here in detail on the basis of the Poisson's ratio. However, the measurement uncertainty for the Young's modulus was calculated according to the same systematic.

A physical variable can be given with  $\bar{x} \pm s_m$  (absolute specification) or  $\bar{x} \pm \frac{s_m}{\bar{x}}$  (relative specification), where  $s_m$  is the measurement uncertainty or the standard error. However, the average Poisson's ratio does not result from a direct averaged measurement but from a function of several, as is shown in Equation (8). Therefore, the Poisson's ratio depends on the average lateral displacement  $\Delta b$ , the average axial displacement  $\Delta l$  and both original average lengths  $l$  and  $b$  ( $\mu_{lb} = f(\Delta b; \Delta l; l; b)$ ).

$$\mu_{lb} = -\frac{\Delta b/b}{\Delta l/l} = -\frac{\Delta b \cdot l}{\Delta l \cdot b} \quad (8)$$

Hence, the uncertainty of the Poisson's ratio requires the calculation of a combined uncertainty using the *Gaussian error propagation law*. Therefore, all individual variables need to be normally distributed [19]. Using the *Shapiro-Wilk-test* this was checked within this work. However, each individual variable given in Equation (8) is in turn also influenced by several factors. In case of the specimen width  $b$  for example, the inaccuracy of the calliper and the staff (the lab assistants who measure and prepare the specimens) already influence the variable. Hence, a combined standard error must already be determined for each individual variable included in Equation (8).

The general *Gaussian error propagation law* is given with:

$$u(X) = \sqrt{\left(\frac{\delta X}{\delta y_1} \cdot u(y_1)\right)^2 + \dots + \left(\frac{\delta X}{\delta y_k} \cdot u(y_k)\right)^2} \quad (9)$$

To determine the combined standard uncertainty of the Poisson's ratio, this equation takes the following form when formulating the partial derivatives:

$$u(\mu) = \sqrt{\left( -\frac{l \cdot \Delta b}{\Delta l \cdot b^2} \cdot u(b) \right)^2 + \left( \frac{l}{\Delta l \cdot b} \cdot u(\Delta b) \right)^2 + \left( \frac{\Delta b}{\Delta l \cdot b} \cdot u(l) \right)^2 + \left( -\frac{l \cdot \Delta b}{b \cdot \Delta l^2} \cdot u(\Delta l) \right)^2} \quad (10)$$

The extended measurement uncertainty is calculated by multiplying the measurement uncertainty from Equation (10) by the coverage factor 1,96, which is often round up to 2,0.

$$U(\mu) = u(\mu) \cdot 2 \quad (11)$$

By indicating the respective extended measurement uncertainty of each test series a range of values is given. With a certainty of 95 % the true average Poisson's ratio lies within this range.

### 3 RESULTS AND DISCUSSION

#### 3.1 PRELIMINARY TESTS

##### 3.1.1 Hygric behaviour of wood as an influence on the Poisson's ratio

First tests consisted of 15 loading and unloading cycles. However, no convergence of the averaged Poisson's ratios was noticeable. The hygric behaviour of wood was considered to be the reason for this since the specimens were measured in another climate after being conditioned at 20°C and 65% r.h.. In order to verify this, comparative tests were performed.

Therefore, six  $\mu_{RT}$ -specimens were stored in two different climates. Three in the climatic chamber and three in the room, where the testing machine was located. The temperature in this measurement room was around 21°C with a relative humidity of approx. 40 %.

In total three comparative tests were performed. Each measurement included two specimens, one that was conditioned in the climatic chamber (CC-specimen) and one that was conditioned in the measurement room (MR-specimen).

All three comparative tests showed very similar results. Figure 8 exemplarily shows one of the resulting graphs.

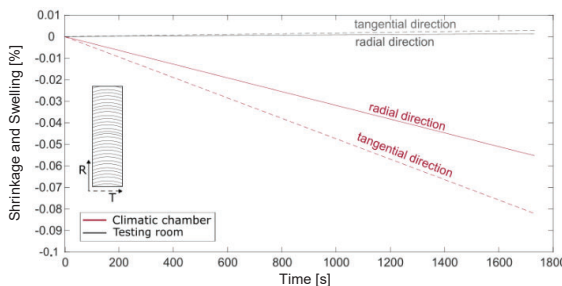


**Figure 8:** Shrinkage and swelling deformations in [%] on the basis of comparative measurements

The specimens conditioned in the climatic chamber show a significantly greater shrinkage in contrast to the specimens conditioned in the measurement room. On the basis of these comparative tests, it is apparent that the change in the ambient climate has a considerable impact measured within one hour after removal from the climatic chamber, as demanded in [11].

Since it was not possible to move the testing machine to the climatic chamber within the scope of this work, all specimens were conditioned in the measurement room.

Figure 9 shows the averaged paths of 15 loading and unloading cycles of two  $\mu_{RT}$ -specimens conditioned in the measurement room and of one specimen conditioned in the climate chamber. This clearly shows that testing the specimens in the same climate in which these were conditioned leads to a significantly lower dispersion. Hence, the shrinkage and swelling effects on the Poisson's ratios could be eliminated to a certain degree. Further, it is evident that the Poisson's ratios of the specimens conditioned and tested in the measurement room are more or less constant over the respective stress range and therefore already show a somewhat linear elastic behaviour. Moreover, a stronger convergence of the cycle paths from the tenth cycle onwards was noticeable for all specimen orientations.

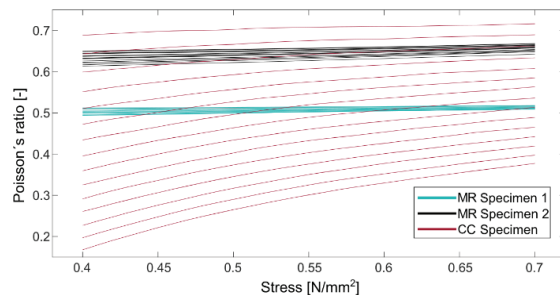


**Figure 9:**  $\mu_{RT}$ -measurements in relation to the stress on the basis of two specimens preconditioned in the measurement room

##### 3.1.2 Impact of creep deformations on the Poisson's ratio

Subsequently it was to be checked if creep deformations had an influence on the test procedure. For this reason, times of constant load of 20 seconds between loading and unloading were included. These were anticipated to lead to a faster convergence of the paths. Therefore, three specimens already tested without times of constant load were tested again including times of constant load within 15 cycles. In addition, three, yet untested specimens were tested including times of constant load. Figure 10 shows the resulting averaged paths for each specimen over the applied stress range.

The specimens measured for the second time including times of constant load show significantly smaller Poisson's ratios than before. This is not inevitably due to creeping but could also be the result of compaction of the specimen during the previous measurements. However, this would also indicate that the linear elastic range had already been exceeded.

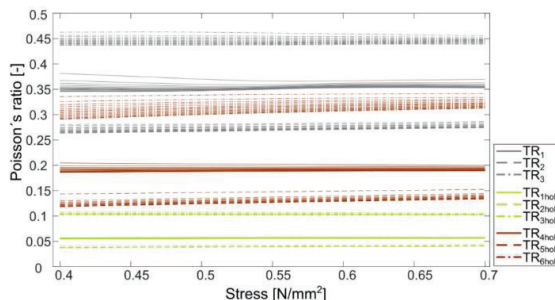


**Figure 10:** Poisson's ratios  $\mu_{TR}$  over stress;  $TR_1$  to  $TR_3$  tested in 15 load cycles without times of constant load;  $TR_{1,hold}$  to  $TR_{3,hold}$  tested with times of constant load;  $TR_{4,hold}$  to  $TR_{6,hold}$  not previously loaded specimens tested with times of constant load

Considering the specimens that were not previously loaded ( $TR_{4,hold}$  to  $TR_{6,hold}$ ) the Poisson's ratios are approximately 30 % lower ( $\mu_{mean,4-6,hold} = 0,213$ ) compared to the specimens tested without constant loads ( $\mu_{mean,1-3} = 0,358$ ). The latter Poisson's ratios measured without times of constant load fit better with the Poisson's ratios measured on spruce wood in previous literature (e.g. [3],[4]).

In conclusion, including times of constant load appears to have an influence on the Poisson's ratios. However, only few tests were carried out here including times of constant load. Similar tests in earlier literature are neither found for compression nor tensile loads. Therefore, the observed results would need to be verified in future studies using a significantly higher number of test specimens. Within this work, times of constant load are omitted.

### 3.1.3 Verification of the linear elastic range

A difficulty often mentioned in previous literature, regarding the Poisson's ratios, was the occurring asymmetry. Therefore, the assumed linear elastic range was checked prior to the main tests. In order to determine if micro cracks with a width of 10-20  $\mu\text{m}$  occur in the assumed linear elastic range, the specimens were scanned before and after loading in a CT-scanner. Due to dimension restrictions only the middle part (30 x 30 x 30 mm<sup>3</sup>) of the specimens was examined. Figure 11 explains the schematic procedure of the CT-measurements. In order to estimate  $F_{c,max}$  two "twin" specimens for each specimen group were taken from the same wooden log at adjacent locations and conditioned in the climate chamber. One of the twins was then loaded till

failure. The other twin was used to detect occurring micro cracks following the procedure shown in Figure 11. In total, due to availability reasons of the CT-scanner, only three specimens were tested.

The comparison of individual sections of the generated 3D model, exemplarily shown in Figure 12, showed no noticeable changes at the micro level after loading the specimens up to 60 % of  $F_{c,max}$  in all three anatomical directions.

In addition, due to availability reasons, only one specimen per load direction was examined. Concluding, the results obtained suggest that the linear elastic range is not exceeded up to 60 % of  $F_{c,max}$ . However, this needs to be verified on the basis of further measurements including a larger number of specimens and if possible, scanning a bigger part of the specimens.

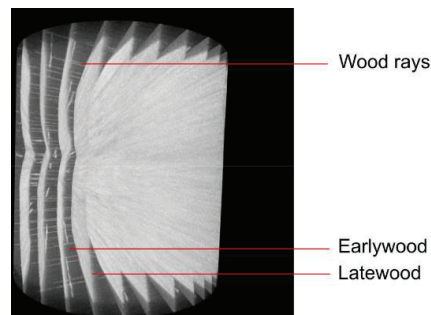


**Figure 12:** Exemplary CT-image of the 3D model of the specimen loaded in the tangential direction

### 3.1.4 Preliminary tests – Conclusion

The preliminary tests resulted in the following conclusions that were applied within the test procedure of the main tests.

- Conditioning of the specimens in the measurement room as the hygroscopicity of wood makes it impossible to measure the Poisson's ratios
- The linear elastic range is verified for all three anatomical directions up to 60 % of  $F_{c,max,est}$ .
- The Poisson's ratio of each test specimen is evaluated in the range between 20 % and 55 % of the respective applied load

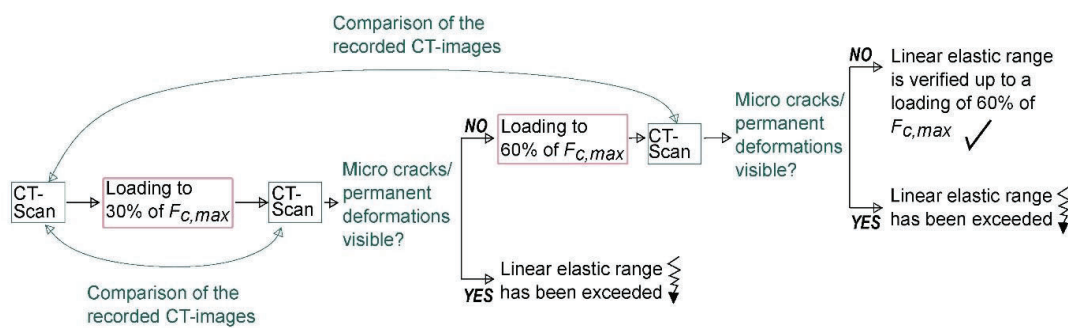


**Figure 11:** Schematic procedure of the CT-measurements and the verification of the linear elastic range of spruce wood

### 3.2 MAIN TESTS

After the test method and handling of samples was defined in several preliminary tests, the main tests were carried out to determine all Poisson's ratios by means of compression tests on spruce wood. The results are shown on the basis of boxplots in Figure 13 and are directly compared to the Poisson's ratios found in literature (square markers, Figure 13). The different colours indicate the respective load types (red: tensile test, blue: compression test and green: bending test) that were applied in literature in order to measure the Poisson's ratios. Table 1 summarizes all Poisson's ratios and Youngs moduli including the measurement uncertainty and the associated average density and wood moisture contents of the respective test series.

Examining the boxplots in Figure 13 it is evident that almost all Poisson's ratios determined in Tripolt [7] and Kumpenza et al. [6] are higher than the ratios determined within this work. Both applied tensile tests and used optical measurement techniques (electronic speckle pattern interferometry (ESPI) and a combination of laser- and videoextensometry). For these measurement techniques, Kumpenza et al. [6] specifies the following measurement resolutions: ESPI 0,03  $\mu\text{m}$ , videoextensometry 0,2  $\mu\text{m}$  and laserextensometry 0,11  $\mu\text{m}$ . The Poisson's ratios in both studies were determined on

specimens with a higher wood moisture content (12 %) than present in this work (~7,4 %, Table 1). Further literature values, determined under the same conditions, though, do not show increased values (see NC [4] in Figure 13). As a consequence, neither the wood moisture content nor the load type appear to be responsible for the increased values. In fact, several indications lead to the assumption that the increased values in Kumpenza et al. [6] and Tripolt [7] resulted from strain measurements during the initial loading of the test specimens. Presumably this has to do with the residual stresses still present during the first loading [4].

This was also evident during the preliminary tests realized in the work presented here.

In case of the  $\mu_{LT}$  values the Poisson's ratios given in Tripolt [7] lie within the inter-quartile range. Presumably, this is due to creep respectively shrinkage effects during capturing the images when using ESPI. That is why Kumpenza et al. did not give any values for  $\mu_{LT}$  [6]. Furthermore, Tripolt mentions difficulties using ESPI on flat sawn where early and late wood alternate and thus, cause inhomogeneous stress conditions [7].

Furthermore, the values determined in Kumpenza et al. [6], using a combination of laser- and videoextensometry, are all higher than the ratios determined within this work. As the strains were only recorded on one side of the specimen using this technique possible bending effects

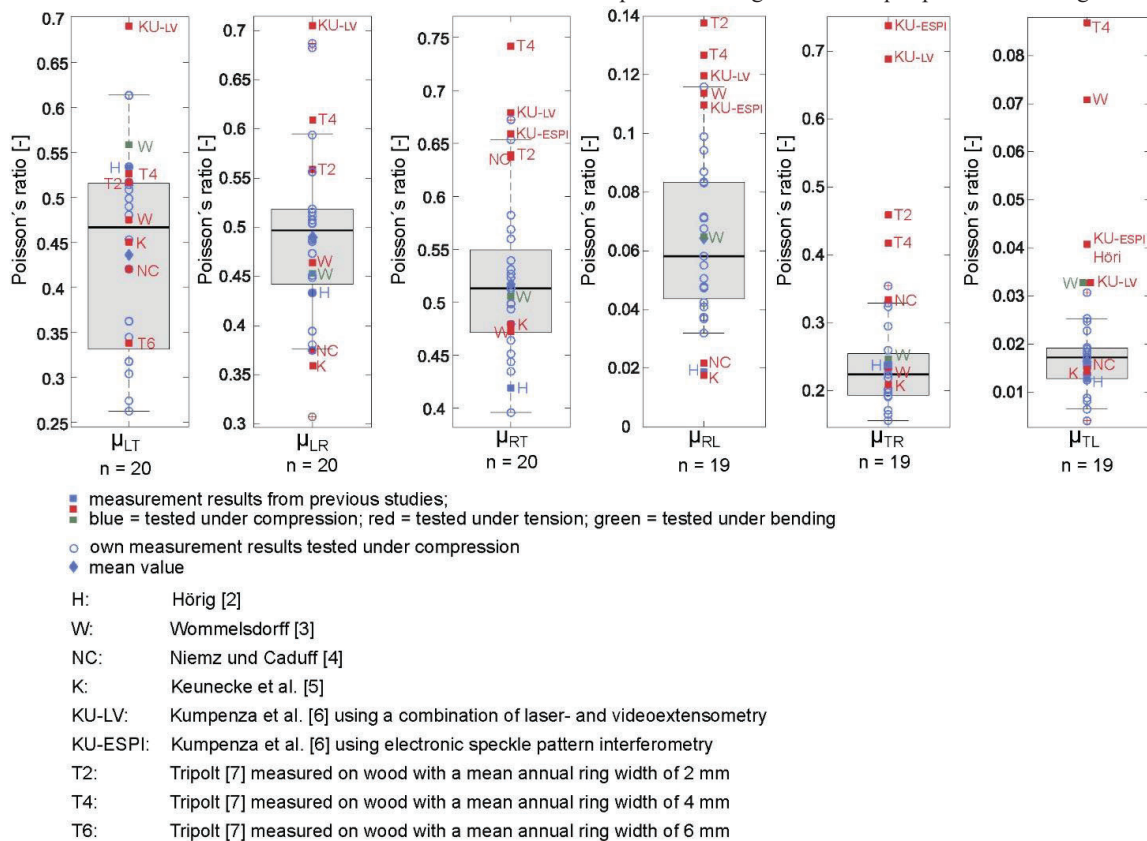


**Figure 13:** Boxplot of the Poisson's ratios of all test series on the basis of  $n$  specimens including the Poisson's ratios determined in previous studies; red: tension tests, blue: compression tests, green: bending tests

were neglected potentially influencing the resulting Poisson's ratios.

A quite good agreement of the values determined within in this work is seen regarding the Poisson's ratios determined in Hörig [2], Wommelsdorff [3], Niemz und Caduff [4] and Keunecke et al. [5]. Here, the test procedure also consisted of several load cycles. Almost all values lie within the inter-quartile range. Only for the RL-series the Poisson's ratios given in [2], [4] and [5] are below this range. It should be mentioned that the Poisson's ratio given in Keunecke et al. [5] is a calculated value and not an outcome of a measurement. However, as already mentioned, the measurement of the lateral strain in longitudinal direction is generally problematic due to the higher stiffness in grain direction. Nevertheless, the Poisson's ratio determined within this work shows a significantly lower deviation ( $\text{CoV} = 38\%$ ) than stated in other studies (e.g.:  $\text{CoV} = 62\%$  [4],  $\text{CoV} = 59\%$  [6]). Moreover, the observed wood moisture contents of around 10 to 12 % given in these references are also higher than present in this work. Since the wood moisture content in radial direction has a greater influence, this might be the reason for the higher deviation of the values. Considering the values for  $\mu_{TL}$  such a deviation cannot be observed which is probably due to the already higher outside temperatures at that time and thus a higher moisture content of around 9,5 % of the specimens. Since the measurement uncertainty has not been a part in previous research further conclusions are difficult to draw.

**Table 1:** Determined Poisson's ratios and Young's moduli including the measurement uncertainty and associated Density, Moisture content and Annual ring width of all test series

Poisson's ratio	[ $-$ ]
$\mu_{RT}$	$0,517 \pm 0,085$
$\mu_{TR}$	$0,233 \pm 0,044$
$\mu_{TL}$	$0,016 \pm 0,005$
$\mu_{LT}$	$0,436 \pm 0,085$
$\mu_{RL}$	$0,064 \pm 0,017$
$\mu_{LR}$	$0,492 \pm 0,123$
Young's moduli	[ $\text{N/mm}^2$ ]
$E_L$	$12068 \pm 1460$
$E_R$	$966 \pm 103$
$E_T$	$302 \pm 42$
Density	[ $\text{kg/m}^3$ ]
$\rho_L$	430
$\rho_R$	428
$\rho_T$	378
Moisture content	[ $\%$ ]
$u_{L,\text{mean}}$	7,4
$u_{R,\text{mean}}$	7,4
$u_{T,\text{mean}}$	9,4
Approx. annual ring width	[mm]
arw	2

Also noteworthy is the resulting Poisson's ratio  $\mu_{RT}$ , that is above 0,5 (Table 1). As a matter of fact, this would indicate that a body under a hydrostatic pressure increases its volume [16]. However, this compressibility condition

is only valid for isotropic materials. Wood is an anisotropic material with different Young's moduli in the three main directions (L,R and T). Therefore, and since Poisson's ratios above 0,5 have also been found in earlier studies, the Poisson's ratio determined for the RT-series is feasible.

The Young's moduli result in the following ratio  $E_T : E_R : E_L$  of  $1 : 3,20 : 39,96$ . For comparison Niemz and Caduff [4] state a ratio of  $1 : 2,43 : 25,4$ , Tripolt [7] a ratio of  $1 : 1,57 : 27,6$ , Kumpenza et al. [6] a ratio of  $1 : 3,69 : 52,08$  and the determined Young's moduli in Keunecke et al. [5] correspond to a ratio of  $1 : 1,57 : 32,24$ . Overall the determined orders of magnitude are therefore in agreement with the literature. The still persistent differences in the ratio of  $E_R : E_T$  can be traced back to the varying annual ring widths [4].

The largest deviation from the literature values is evident regarding the Young's modulus  $E_T$ . This test series also shows a significantly lower density value and the highest moisture content. A possible reason for the lower density might be the small sample geometry combined with the annual ring width [4]. Since the Young's modulus decreases with lower density [20], this might be the reason for the deviation. The lower moisture content of 9,4% compared to the literature values (~12%) should cause a higher Young's modulus. Compared to the influence of the density, however, this seems to have less impact on the Young's modulus.

### 3.2.1 Symmetry condition

When summarizing all obtained values and inserting these into the compliance matrix, the matrix should fulfil the symmetry condition.

$$\begin{bmatrix} \frac{1}{E_L} & -\frac{\mu_{RL}}{E_R} & -\frac{\mu_{TL}}{E_T} \\ -\frac{\mu_{LR}}{E_L} & \frac{1}{E_R} & -\frac{\mu_{TR}}{E_T} \\ -\frac{\mu_{LT}}{E_L} & -\frac{\mu_{RT}}{E_R} & \frac{1}{E_T} \end{bmatrix} = \begin{bmatrix} \frac{1}{12068} & -\frac{0,064}{966} & -\frac{0,016}{302} \\ -\frac{0,492}{12068} & \frac{1}{966} & -\frac{0,233}{302} \\ -\frac{0,436}{12068} & -\frac{0,517}{966} & \frac{1}{302} \end{bmatrix} \quad (12)$$

$$= \begin{bmatrix} 8,29 & -6,63 & -5,3 \\ -4,08 & 103,52 & -77,15 \\ -3,61 & -53,52 & 331,13 \end{bmatrix} \cdot 10^{-5}$$

It is seen, that at first glance, based on the presented compliance matrix in Equation (12) the symmetry condition is not identified as fulfilled. This is why the determined measurement uncertainties are additionally considered in the following. Thereby, the symmetry conditions are examined individually.

First symmetry condition:

$$\begin{aligned} \frac{\mu_{LR}}{E_L} &= \frac{\mu_{RL}}{E_R} \\ 0,492 \pm 0,123 &= 0,064 \pm 0,017 \\ 12068 \pm 1460 &= 966 \pm 103 \\ [2,73; 5,88] \cdot 10^{-5} &= [4,40; 9,39] \cdot 10^{-5} \end{aligned} \quad (13)$$

with: [ $\min$ ;  $\max$ ]. This results in an overlapping area of  $5,8 \cdot 10^{-5} - 4,4 \cdot 10^{-5} = 1,4 \cdot 10^{-5}$ . Therefore, the symmetry condition can theoretically be fulfilled if both values lie within this range. Since the true average

Poisson's ratio and the true Young's modulus lie in the respective range with a 95 %-confidence, both values lie in the overlap range with a confidence of approx. 12 %. Following this example, the second symmetry condition (Equation (14)) is theoretically met on a confidence level of approx. 20 % and the third symmetry condition (Equation (15)) is met on a confidence level of approx. 13 %.

$$\frac{\mu_{LT}}{E_L} = \frac{\mu_{TL}}{E_T} \quad (14)$$

$$\frac{\mu_{RT}}{E_R} = \frac{\mu_{TR}}{E_T} \quad (15)$$

In general, it can therefore be assumed that the compliance matrix determined here corresponds to the symmetry requirement. This supports the developed testing method and the applied measurement technique. The matrix given in Equation (12) can then take the following symmetrical form and may be applied in the context of FEM.

$$\begin{bmatrix} 8,29 \cdot 10^{-5} & -5,14 \cdot 10^{-5} & -4,11 \cdot 10^{-5} \\ -5,14 \cdot 10^{-5} & 1,04 \cdot 10^{-3} & -6,24 \cdot 10^{-4} \\ -4,11 \cdot 10^{-5} & -6,24 \cdot 10^{-4} & 3,31 \cdot 10^{-3} \end{bmatrix} \quad (16)$$

#### 4 CONCLUSION AND OUTLOOK

This paper takes the extended measurement uncertainty into account. As a result, the six determined average Poisson's ratios can be stated with a 95 %-confidence. The results obtained seem to be consistent, since the average values lie in the middle range of the results stated in literature. This also includes the Young's moduli and the density values.

However, it was seen that measurements based on the first loading, lead to significantly higher Poisson's ratios due to residual stresses. Within future studies it is therefore particularly important to provide more precise information on the test and load procedure. In this context, it is of interest whether measurements using ESPI or a combination of laser- and videoextensometry result in similar Poisson's ratios as found within this work, when determining the Poisson's ratio based on the 10<sup>th</sup> load cycle.

Besides the load procedure, it also appears that the one- or two-sided measurements of the strains on a specimen influence the results. On the one hand this can be concluded from the values determined using laser- and videoextensometry in [6]. There, the strains were determined on only one side of the specimen and are above the determined average in all test series. On the other hand, a measurement on a  $\mu_{TL}$ -specimen in this work caused an extremely high Poisson's ratio. This is why this measurement was eliminated within the evaluation here. Reason for this increased Poisson's ratio was most likely the fact that one of the strain gauges was defective. Thus, the lateral strain was only recorded on one side of the specimen here as well.

Additionally, it should be pointed out, that measuring  $\mu_{TL}$  and  $\mu_{LT}$  by means of optical measurement techniques is rather impractical. Difficulties due to different proportions of early- and latewood on the measuring surface were mentioned for example in [7]. Considering that these values, given in Tripolt [7] deviate significantly from the values determined here, this can be confirmed on the basis of this paper.

What could not be confirmed within the present thesis is the stress dependence of individual Poisson's ratios found in [3]. Prerequisite for an accurately constant Poisson's ratio and thus a stress independent Poisson's ratio is the accurately linear progression of the axial and lateral strain. On a random basis a linear regression was carried out on these strains over the stress. In each case, the strains run linearly, however, not perfectly. The resulting smallest deviations lead to a deviation of the Poisson's ratio over the stress. As a consequence the partial stress dependence is more an artefact of the measurement fluctuations or measurement uncertainty than an actual stress dependence. This should be verified in detail in future studies, as the above finding is only based on a small sample number. In case it turns out that measurement fluctuations and the measurement uncertainty are not the reason for the partly recognisable stress dependence, the assumption of a rhombic-crystalline behaviour of wood would have to be rejected, as was already mentioned by Wommelsdorff [3].

The present results of the preliminary tests further confirm that in the event of future studies investigating the influence of wood moisture on the Poisson's ratios, special care needs to be taken to perform the measurements in the same climate in which the specimens are conditioned. Otherwise, shrinkage and swelling influences have already a considerable influence on the Poisson's ratios within a short time period.

Significant correlations were only evident in a few cases. Moreover, these often differ from the correlations found in [7]. In addition, the Poisson's ratios are not only dependent on the density and the Young's modulus, but also on the microfibril angle and the cell shape angle [21]. These parameters were not recorded within the scope of this paper. Future studies should therefore examine correlations using a larger number of specimens and taking into account more wood properties such as the microfibril angle, the cell shape angle, etc..

Furthermore, creep also seems to have an influence on the measurement results of the Poisson's ratio, as is apparent from the preliminary tests. In this context, it seems reasonable to determine Poisson's ratios including the creep influence in future studies. These could be of particular importance for components subjected to long-term stress.

In summary, the determination of extended Poisson's ratios of spruce wood has been achieved by integrating the measurement uncertainty. From an engineering perspective subsequent research should validate the Poisson's ratios determined on clear wood specimens. For this purpose, a combination of finite element method (FEM) calculations in conjunction with associated

measurements on component-sized specimens suggests itself.

## ACKNOWLEDGEMENT

This paper is based on my Master's thesis [22] which I was able to write in cooperation between the Technical University of Munich and the University of Innsbruck, supervised by my Co-Authors. Additionally, I would like to thank Dr.-Ing. Patrik Aondio for his support throughout the thesis. Furthermore, I want to acknowledge the entire TVFA team of the University of Innsbruck, without whom I would not have been able to conduct all the measurements. At this point additional thanks go to the Unit of Material Technology at the University of Innsbruck, that enabled the CT-measurements.

## REFERENCES

- [1] Stamer, J. (1935). Elastizitätsuntersuchungen an Hölzern. *Ingenieur-Archiv*, 6(1), 1–8. <https://doi.org/10.1007/BF02086406>
- [2] Hörig, H. (1935). Anwendung der Elastizitätstheorie anisotroper Körper auf Messungen an Holz. *Ingenieur-Archiv*, 6(1), 8–14. <https://doi.org/10.1007/BF02086407>
- [3] Wommelsdorff, O. (1966). *Dehnungs- und Querdehnungszahlen von Hölzern*. Technische Hochschule Hannover, Hannover.
- [4] Niemz, P., & Caduff, D. (2008). Untersuchungen zur Bestimmung der Poissonschen Konstanten an Fichtenholz. Holz als Roh- und Werkstoff, 66(1), 1–4. doi: 10.1007/s00107-007-0188-2
- [5] Keunecke, D., Hering, S., & Niemz, P. (2008). Three-dimensional elastic behaviour of common yew and Norway spruce. *Wood Science and Technology*, 42(8), 633–647. <https://doi.org/10.1007/s00226-008-0192-7>
- [6] Kumpenza, C., Matz, P., Halbauer, P., Grabner, M., Steiner, G., Feist, F. et al. (2018). Measuring Poisson's ratio: mechanical characterization of spruce wood by means of non-contact optical gauging techniques. *Wood Science and Technology*, 52(6), 1451–1471. <https://doi.org/10.1007/s00226-018-1045-7>
- [7] Tripolt, M. (2018). *Prüftechnische Bestimmung des orthotropen Elastizitätsverhaltens von Fichtenholz*. Masterarbeit. Technische Universität Graz, Graz.
- [8] Clauß, S., Pescatore, C., & Niemz, P. (2014). Anisotropic elastic properties of common ash (*Fraxinus excelsior L.*). *Holzforschung*, 68(8), 941–949. <https://doi.org/10.1515/hf-2013-0189>
- [9] DIN 52185. (1976-09). Bestimmung der Druckfestigkeit parallel zur Faser. Berlin: Deutsches Institut für Normung e.V. Beuth Verlag GmbH.
- [10] DIN 52192. (1979-05). Druckversuch quer zur Faserrichtung. Berlin: Deutsches Institut für Normung e.V. Beuth Verlag GmbH.
- [11] EN 408. (2012-10). Holzbauwerke - Bauholz für tragende Zwecke und Brettschichtholz: Bestimmung einiger physikalischer und mechanischer Eigenschaften. Berlin: Deutsches Institut für Normung e.V. Beuth Verlag GmbH.
- [12] EN 338. (2016-07). Bauholz für tragende Zwecke: Festigkeitsklassen. Berlin: Deutsches Institut für Normung e.V. Beuth Verlag GmbH.
- [13] EN 12390-13. (2013-12). Prüfung von Festbeton: Teil 13: Bestimmung des Elastizitätsmoduls unter Druckbelastung (Sekantenmodul). Wien: Austrian Standards plus GmbH.
- [14] Bodig, J. & Jayne, B. A. (1982). Mechanics of wood and wood composites. New York: Van Nostrand Reinhold
- [15] Mang, H. A., Hofstetter, G. & Eberhardsteiner, J. (2013). *Festigkeitslehre* (Lehrbuch, 4., erw. Aufl.). Berlin, Heidelberg: Springer Vieweg Verlag.
- [16] Grimsel, M. (1999). Mechanisches Verhalten von Holz. Struktur- und Parameteridentifikation eines anisotropen Werkstoffes (Dresdner Forschungen Maschinenwesen, Bd. 1). Dresden: w.e.b.-Univ.-Verl.
- [17] Albers, K. (1970). Querdehnungs- und Gleitzahlen sowie Schub- und Scherfestigkeiten von Holzwerkstoffen. Dissertation. Universität Hamburg, Hamburg.
- [18] Niemz, P., & Sondergger, W. U. (2017). *Holzphysik: Physik des Holzes und der Holzwerkstoffe: mit zahlreichen Bildern und Tabellen*. München: Fachbuchverlag Leipzig im Carl Hanser Verlag. Retrieved from <http://www.hanser-fachbuch.de/9783446445260>
- [19] Maul, C., & Dammeyer, T. (2012). *Apparatives Praktikum Physikalische Chemie der TU Braunschweig: Messfehler, Fehlerberechnung und Fehlerabschätzung*. Technische Universität Braunschweig. Braunschweig.
- [20] Neuhaus. (2017). *Ingenieurholzbau*. Springer Fachmedien Wiesbaden.
- [21] Qing, H., & Mishnaevsky, L. (2010). 3D multiscale micromechanical model of wood: From annual rings to microfibrils. *International Journal of Solids and Structures* (47), 1253–1267. Retrieved from <https://www.sciencedirect.com/science/article/pii/S0020768310000259?via%3Dihub>
- [22] Winter, K. (2021). A new Approach to Determine and Evaluate the Poisson's Ratio of Spruce Wood. Masterarbeit. Technical University of Munich & University of Innsbruck. Munich